

## Eccentric Disks from Circumbinary Rings

LEONARDO BETANCOURT ,<sup>1,2</sup> ANDREW MACFADYEN ,<sup>1</sup> AND JONATHAN ZRAKE ,<sup>3</sup>

<sup>1</sup>Center for Cosmology and Particle Physics, Physics Department, New York University, New York, NY 10003, USA

<sup>2</sup>Department of Astronomy, California Institute of Technology, 1200 East California Boulevard, Pasadena, CA 91125, USA

<sup>3</sup>Department of Physics and Astronomy, Clemson University, Clemson, SC 29634, USA

### ABSTRACT

We perform high-resolution, grid-based hydrodynamics simulations of finite gaseous circumbinary rings (CBRs) viscously spreading into disks around binaries. We find that all systems suppress accretion onto the binary when the gas is relatively cold. CBRs display weak variability above the binary orbital frequency  $\Omega_b$  and a dominant, robust spectral peak at  $\sim 0.1\Omega_b$  (half the fiducial lump frequency of  $\sim 0.2\Omega_b$ ). Smaller rings relax into disks with enhanced gas eccentricity up to  $e \simeq 0.3$ . We consider the possibility that inefficiently-accreting, intermediate-mass ( $\sim 10^4 M_\odot$ ) black hole binaries may be sources of quasi-periodic eruptions when rejected streams shock the cavity wall and radiate in the UV or soft X-ray. We discuss the implications of eccentric disks evolved from CBRs for quasar light curves and asymmetric, time-variable double-peaked line emission from disks in galactic nuclei. If binaries drive asymmetry in accretion disk line profiles, our study suggests that the progenitor CBR must have been very compact.

*Keywords:* Accretion Disks (xxx) — Binaries (xxx) — Supermassive black holes (xxx) — Tidal disruption events (xxx)

### 1. INTRODUCTION

Binary star and black hole systems are expected, on observational and theoretical grounds, to be ubiquitous. Spectroscopic surveys (Duquennoy & Mayor 1991) as well as astrometric measurements (Raghavan et al. 2010; El-Badry et al. 2021) suggest that a large number of stars, and the majority of solar-like stars, exist in pairs or higher-order multiples (see Duchêne & Kraus 2013 for review). During hierarchical structure formation, galaxy mergers are expected to frequently produce super-massive black hole binaries (SMBHBs) at their centers. Their existence is supported by both analytic (Begelman et al. 1980; Volonteri et al. 2003; Merritt & Milosavljević 2005; Dosopoulou & Antonini 2017), and numerical (Dotti et al. 2007; Qian et al. 2024) studies which demonstrate that dynamical friction against the gaseous background causes the black holes to migrate to the galactic center, shrinking their orbital separation down to the parsec scale.

Recent cosmological simulations have shown that the time-dependent potential of the binary may produce alternative circumbinary gas morphologies with fundamental differences to the fiducial extended disk model (Muñoz et al. 2019, Duffell et al. 2024). For instance,

Goicovic et al. (2016) showed that low-angular momentum clumps of gas from the interstellar medium can form nearly-circular rings of gas around a binary as a result of their near-radial infall. These rings have radii on the order of the binary separation and have been shown to form with random angular momentum vectors with respect to that of the binary, including both prograde and retrograde configurations. Similarly, numerical simulations of tidal disruption events (TDEs) suggest the formation of rings around SMBHBs when a star falls below either BH's tidal radius (Coughlin et al. 2016; Coughlin et al. 2017; Ryu et al. 2022; Yu & Lai 2025).

Circumbinary rings are not limited to massive black holes binaries, but also form around binary star systems. It is widely believed that stellar disks accrete too slowly to account for the growth rate of stars inferred from observation. This suggests that stars most likely form in clusters, where turbulent gas can create misaligned accretion flows that effectively cancel their angular momenta and accrete more promptly (Bate et al. 2003; Grudić et al. 2022). In addition, hydrodynamics studies have shown that gas rings form as stars collide with this chaotic accretion flow and form binaries (Borchert et al. 2022). Ring accretion may have also been observed in ALMA studies of protoplanetary structures. For exam-

ple, [Guerra-Alvarado et al. \(2025\)](#) found that two-thirds of stellar systems in Lupus are surrounded by compact dust structures, some in ring-like shapes with radii as small as 0.6 au. Though it remains unclear whether any are binaries, it is likely given that these stars form in turbulent clusters.

Recent hydrodynamic studies have discovered a regime of suppressed accretion in the limit of a thin disk,  $h/r \sim \mathcal{M}^{-1} \lesssim 0.025$  where  $\mathcal{M}$  is the orbital Mach number ([Ragusa et al. 2016](#); [Dittmann & Ryan 2022](#); [Tiede et al. 2025](#)). These models, however, assume an ‘infinite’ disk that extends far out from the binary, and it remains to be studied whether suppressed accretion is sensitive to finite-disk effects. [Muñoz et al. \(2020\)](#) studied accretion from both finite tori and infinite disks, finding that both disk configurations exert similar torques on the binary. Here, we extend their analysis to determine whether the suppressed accretion regime is robust with respect to disk extent.

We perform high-resolution hydrodynamics simulations of a viscous ring of gas as it relaxes into an accretion disk around a binary over multiple viscous timescales  $t_{\text{visc}} \sim R_0^2/\nu$ , where  $R_0$  is the initial ring radius and  $\nu$  is the kinematic viscosity. Since all of our simulations are scale-free, our findings are applicable to both stellar and black hole binaries.

This Letter is organized as follows. In Section 2, we detail the initial conditions and numerical methods employed to run our suite of simulations. In Section 3, we compare accretion signatures between circumbinary gas models. In Section 4, we report on the growth and saturation of the disk eccentricity and its dependence on our simulation parameters  $R_0$ ,  $\mathcal{M}$  and disk extent. In Section 5, we discuss the observational implications of our results in the context of EM-dark binaries in quasars, quasi-periodic eruptions from galactic centers and double-peaked line emission from accretion disks. In Section 6, we summarize our findings.

## 2. NUMERICAL SETUP

A gaseous disk surrounds an equal-mass ( $q_b = M_2/M_1 = 1$ ), circular binary ( $e_b = 0$ ) with total mass  $M$  and semimajor axis  $a$ . The disk is locally isothermal and geometrically thin with orbital Mach number  $\mathcal{M} \sim (h/r)^{-1} \gg 1$ . Viscous stresses are implemented via a constant- $\nu$  viscosity prescription  $\nu = \bar{\nu} a^2 \Omega_b$  and  $\bar{\nu} = 10^{-3}$ , where  $\Omega_b$  is the binary orbital frequency. Accretion onto each binary component is modeled via torque-free sink terms which remove mass and momentum from the computational domain (see [Dempsey et al. 2020](#)). This is the standard circumbinary setup described in [Duffell et al. \(2024\)](#) with a modified initial

surface density. The gas is initialized as a ring of radius  $R_0$  and width  $\sigma = 0.1R_0$ , implemented with a Gaussian radial profile,

$$\Sigma(r) = \Sigma_0 e^{-(r-R_0)^2/2\sigma^2}, \quad (1)$$

where  $\Sigma_0$  is set such that the initial mass of the ring  $M_{\text{ring}} = 1$ . Note that this is purely for convenience in post-processing, since we implicitly assume  $M_{\text{ring}} \ll M$  by ignoring self-gravity. We impose a surface density floor of  $\Sigma/\Sigma_0 \geq 10^{-10}$  throughout the simulation. Tests with several alternative floor values show that this choice ensures numerical stability without affecting the hydrodynamic evolution.

We run a total of 25 simulations comparing ring and disk initial conditions. We perform 20 ring simulations exploring radii  $R_0 = \{1a, 2a, 3a, 4a\}$  and orbital Mach numbers  $\mathcal{M} = \{10, 20, 30, 40, 60\}$ . For direct comparison between ring and infinite disk, we run an additional suite of 5 infinite disk simulations at constant- $\nu$  viscosity and equivalent Mach numbers.

The computational domain is square with side lengths  $30a$  (ring) and  $24a$  (infinite disk) and uses Cartesian coordinates. The resolution is uniform with  $\Delta x = 0.01a$ . The simulations are performed using [Meena](#), a second-order, GPU-accelerated Godunov hydrodynamics code written in JAX ([Bradbury et al. 2018](#)) by the lead author.

## 3. ACCRETION DYNAMICS

### 3.1. Suppressed Accretion

In the initial transient period, all rings studied become tidally disrupted by the binary potential. Gas in the outer ring spreads radially outward, while gas in the inner edge is pulled into streams, leading to capture by either binary component or flinging of the stream back out to the edge of the cavity (the central region around the binary containing very low density of fluid; [MacFadyen & Milosavljević 2008](#)). While the ring exhibits complex angular momentum redistribution during this transient period, we focus on the feeding dynamics of a relaxed disk evolved from a ring initial condition.

Figure 1 compares quasi-steady-state accretion rates of the ‘infinite’ disk and the  $R_0 = 4a$  ring following the initial transient period. After a viscous time, we observe the relaxed ring to accrete at a rate that decreases as it is secularly depleted ([Muñoz et al. 2020](#)). Due to this depletion on the viscous timescale, we normalize the reported accretion rates by the time-dependent mass of the ring to make a fair comparison between simulations. In the disk case,  $M$  is normalized by the large-scale inflow rate,  $\dot{M}_\infty = 3\pi\Sigma_0\nu a^2\Omega_b$  (see [Tiede et al. 2025](#)). In the top panel of Figure 1, we recover the accretion suppression observed previously in the limit of a thin

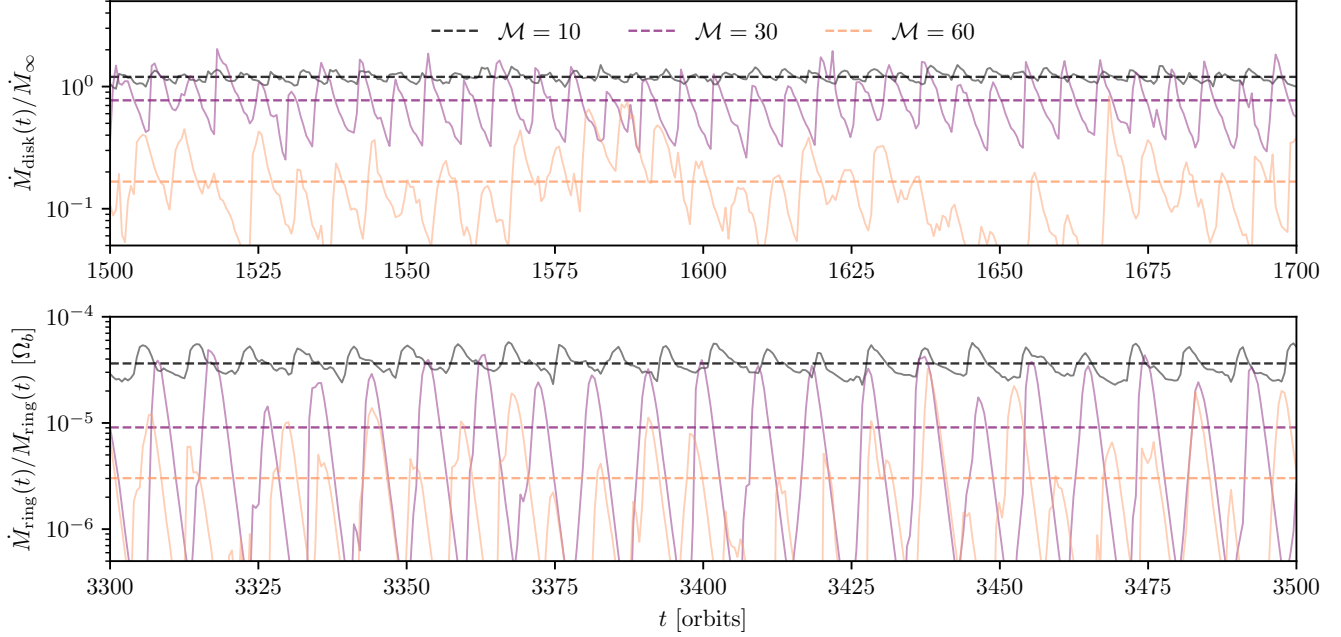


**Figure 1.** (Top) Accretion rate timeseries of the infinite disk in quasi-steady-state, normalized by the large-scale inflow rate,  $\dot{M}_{\infty} = 3\pi\Sigma_0\bar{\nu}a^2\Omega_b$ . (Bottom) Accretion rate timeseries of the  $R_0 = 4a$  ring well after  $t_{\text{visc}}$ . In both plots, the dashed lines represent the time-averaged normalized accretion rates.

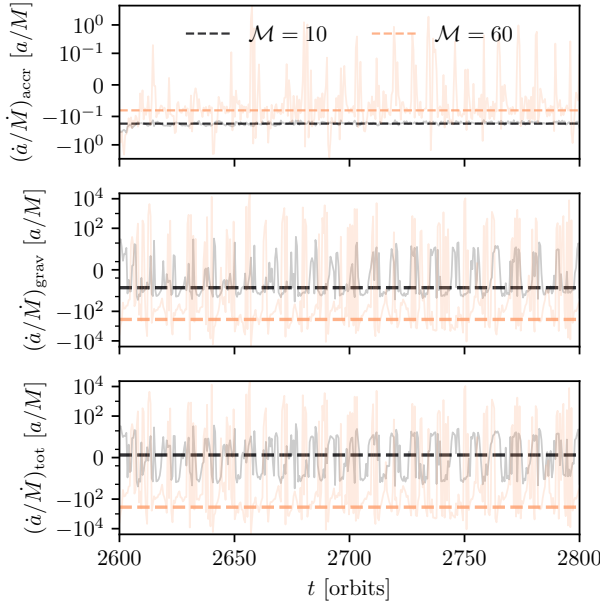


**Figure 2.** Accretion (top), gravity (middle), and total (bottom) contributions to the time-derivative of the binary semi-major axis  $a$ .

infinite disk, where the  $\mathcal{M} = 60$  disk accretes at a rate  $\sim 10\%$  of the  $\mathcal{M} = 10$  disk. The time-averaged accretion rates decrease monotonically with increasing  $\mathcal{M}$ . The bottom panel shows a very similar suppression fac-

tor in the relaxed ring of relatively cold ( $\mathcal{M} = 60$ ) gas. This suggests that accretion dynamics are insensitive to large-scale gas structure and are instead driven largely by interaction between the binary and the cavity inner edge. In other words, the efficiency of stream capture decreases dramatically in colder gas, regardless of initial condition.

Figure 2 shows the individual contributions to the evolution of the binary separation  $\dot{a}$ , as well as their combined effect. For an equal-mass binary, this rate is given by

$$\frac{\dot{a}}{\dot{M}} = 2 \left( \frac{\ell_0}{\ell} - \frac{3}{2} \right) \frac{a}{M}, \quad (2)$$

where  $\ell_0 \equiv \dot{L}/\dot{M}$  is the total torque on the binary normalized by the accretion rate and  $\ell \equiv L/M$  is the specific angular momentum of the binary. Figure 2 shows that the evolution of the binary separation is dominated by gravitational torques. In colder disks, streams of gas are more likely to miss the binary, effectively stealing specific angular momentum on the order of  $a^2\Omega_b$  with each binary encounter (Tiede et al. 2025). The result is that cold disks and rings alike push the binary closer together, with increasingly colder gas driving faster inspiral.

In comparison with previous studies by Tiede et al. (2025), we find that the level of suppression is sensitive to the viscosity prescription in the disk. Tiede et al.

(2025) showed  $\alpha$ -disks with  $\bar{\nu} = 10^{-4}$  to exhibit a  $\sim 1\%$  suppression between  $\mathcal{M} = 10$  and  $\mathcal{M} = 60$ , while our findings suggest a  $\sim 10\%$  suppression factor. However, since accretion disks are likely much thinner, in the range  $h/r \sim \mathcal{M}^{-1} \sim 10^{-2} - 10^{-3}$  (Shakura & Sunyaev 1973), the astrophysical consequences are robust. Cold CBDs may produce reduced accretion-driven electromagnetic luminosity, regardless of their radial extent.

### 3.2. Accretion Periodicity

As the tidal potential drives an eccentric instability in the cavity, periodic ‘lump’ accretion emerges. Rejected streams pile up coherently on the opposite edge of the cavity wall, producing an over-density that delivers mass to the binary at a certain frequency (Lubow 1991; MacFadyen & Milosavljević 2008; Shi et al. 2012). Figure 3 shows 25-orbit timeseries of the accretion rate, which is modulated by this periodic signal. At  $\mathcal{M} = 10$ , the circumbinary ring produces the familiar sawtooth accretion pattern observed previously in simulations of the infinite disk. For higher  $\mathcal{M}$ , however, we observe accretion signatures that differ depending on initial conditions. In the infinite disk, the sawtooth pattern is robust for varying  $\mathcal{M}$ . In the ring, accretion flares become significantly more symmetric and are closer to triangular wave patterns as  $\mathcal{M}$  increases. Figure 3 also demonstrates the discrepancy in accretion flare amplitudes associated with suppressed ‘lump’ delivery for  $\mathcal{M} = 60$ . Inefficiency of stream capture at  $\mathcal{M} = 60$  makes the overdensity more likely to miss the binary if it hasn’t yet accumulated enough gas from rejected streams.

In the fiducial CBD, ‘lump’ accretion episodes occur at a frequency of  $\sim 0.2\Omega_b$  (every  $\sim 5$  binary orbits; MacFadyen & Milosavljević 2008). We observe a weak dependence of this dominant frequency on  $\mathcal{M}$ , with higher  $\mathcal{M}$  disks exhibiting slightly lower ‘lump’ frequencies. In the circumbinary ring, the dominant frequency is significantly lower, at  $\sim 0.1\Omega_b$ . Unlike the infinite disk, this dominant frequency appears to be largely insensitive to  $\mathcal{M}$ .

Beyond the dominant frequency, the character of the periodograms differ significantly between initial conditions. In the infinite disk, subdominant frequencies at  $\sim 0.4\Omega_b$  and  $\sim 2\Omega_b$  become lost to noise for higher  $\mathcal{M}$ , with  $\mathcal{M} = 60$  exhibiting approximately constant power for all frequencies above the dominant peak. In the ring, these subdominant frequencies appear much weaker, and their strength diminishes for higher  $\mathcal{M}$ . At  $\mathcal{M} \gtrsim 40$ , frequency noise above the dominant frequency has two orders of magnitude less power than the infinite disk at equivalent  $\mathcal{M}$ . Thus, CBRs exhibit significantly cleaner

periodicity with a single dominant mode at  $\sim 0.1\Omega_b$  and accretion variability with a quasi-triangular shape.

## 4. DISK ECCENTRICITY

CBDs are generally susceptible to the eccentric-cavity instability (ECI). This instability is driven in part by rejected streams impacting the CBD wall (see Sec. 4.3.3 in Shi et al. 2012). The instability can thus be arrested by gas capture to the holes, by reducing the strength of the rejected stream impacts. The larger-scale CBD can also play a role in quenching the ECI, either by absorbing or helping to dissipate the excess orbital energy of the inner CBD gas. Thus larger disks are generally expected to saturate at a smaller eccentricity.

We measure the radial distribution of the gas eccentricity, where each Fourier component is defined as

$$\tilde{e}_m \sim \frac{|\langle \Sigma v_r e^{im\phi} \rangle|}{\langle \Sigma v_\phi \rangle}, \quad (3)$$

and we report the first two components added in quadrature,  $e = (\tilde{e}_1^2 + \tilde{e}_2^2)^{1/2}$ . Figure 4 shows the distribution of  $e$  binned by the semi-major axis of the gas orbits,  $a_{\text{gas}} = -GM/2\epsilon$ , where  $\epsilon$  is the gas specific orbital energy. We observe gas in cold, infinite disks to remain in largely circular orbits independent of  $\mathcal{M}$ . Cold rings, on the other hand, exhibit dramatically higher gas eccentricity for  $\mathcal{M} \rightarrow 60$ . Figure 4 also demonstrates that smaller rings ( $R_0 \rightarrow 1a$ ) evolve to disks with significantly higher eccentricity. For ring  $R_0 = 1a$  at  $\mathcal{M} = 60$ , the majority of circumbinary gas settles in orbit with semi-major axis  $a_{\text{gas}} \gtrsim 6a$  and eccentricity  $e \gtrsim 0.2$ , and a significant portion of gas orbits with  $e \simeq 0.3$ . This is consistent with measurements of accretion suppression, as the inefficiency of gas capture causes rejected streams to transfer excess orbital energy to the inner CBD, thereby growing the gas eccentricity. We therefore find that, in the limit of relatively warm rings ( $\mathcal{M} \simeq 10$ ) of large initial radius ( $R_0 \gtrsim 4a$ ), circumbinary dynamics evolve towards the fiducial infinite disk model. In the limit of cold rings ( $\mathcal{M} \gtrsim 60$ ) of small initial extent ( $R_0 \simeq 1a$ ), the binary drives significant eccentricity growth in the relaxed disk.

While measurements of accretion rates (Figure 1) suggest that accretion suppression is robust to varying gas distribution, the outer CBD does appear to influence the orbital dynamics of the circumbinary gas. We posit that the suppression of the ECI can be understood by modeling the outer CBD as an infinite Keplerian reservoir of angular momentum. In cold disks, tidal streams pulled from the cavity edge lack pressure support and as a result are spread thinner by gravitational forces. These thin streams are less efficiently captured and end

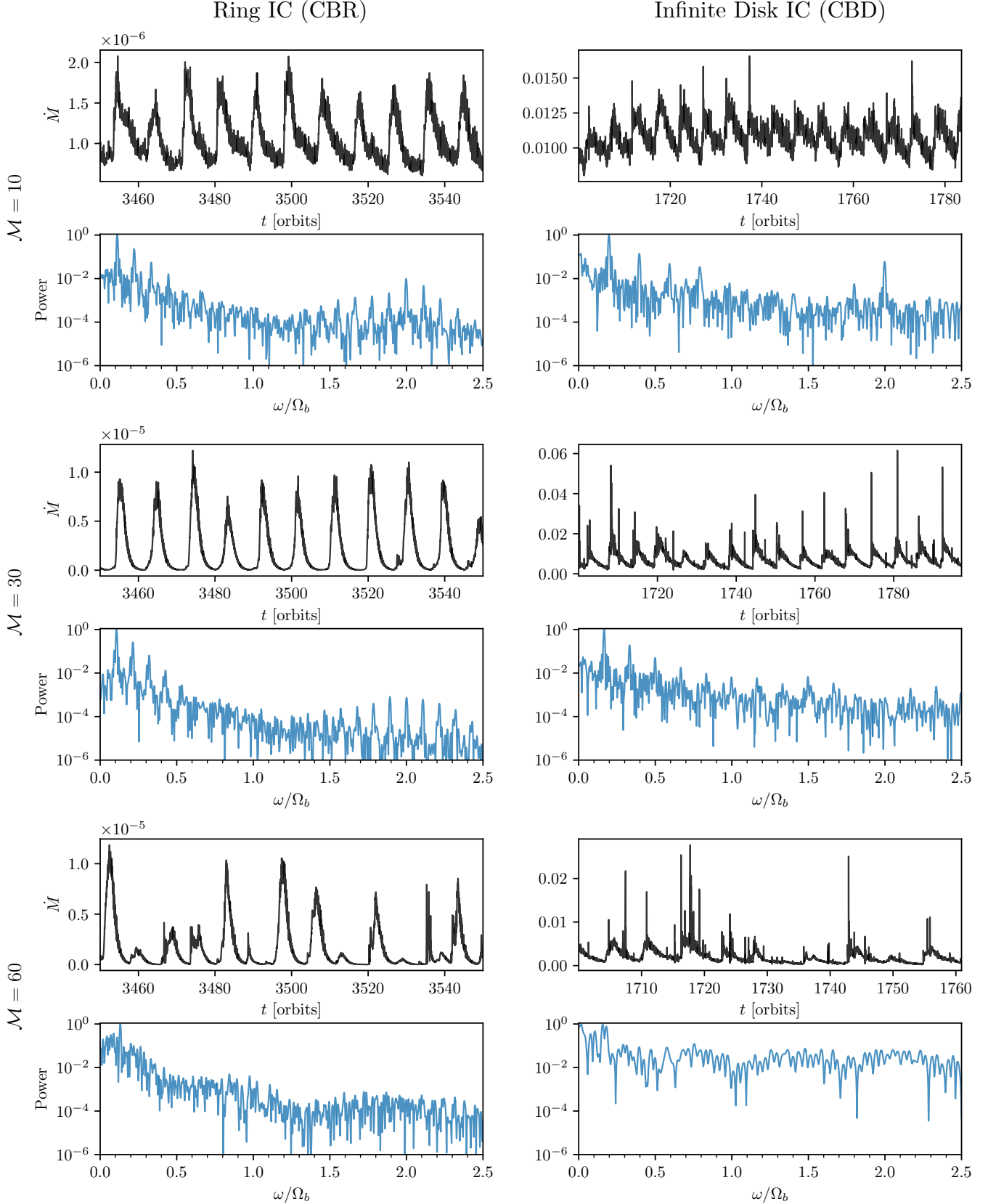


**Figure 3.** 100-orbit windows of the accretion rate (top) and the corresponding Lomb-Scargle periodogram (bottom) computed over 100 orbits in quasi-steady-state. Left and right panels compare ring and infinite disk initial conditions (ICs) respectively.

up missing the binary. Thus the tidal encounter concludes when the gas is kicked up by the binary potential with enhanced orbital energy. As the inner CBD gains orbital energy from rejected streams, this is reconciled with the available supply of angular momentum from the outer disk; gas re-equilibrates to larger circular orbits. A ring lacks an outer CBD for this process, so gas orbits grow to higher eccentricity as streams impact the cavity wall (Figure 4).

## 5. DISCUSSION

### 5.1. *Binary Periodicity*

The dominant source of EM variability in circumbinary gas systems is believed to originate in the inner disk, where tidal streams deliver gas to each component and accrete through minidisks (Cocchiararo et al. 2024). Detecting such flux variability, assumed to be closely tied to the rate of accretion, may allow us to infer the binary’s orbital period and spatial separation. The associated frequency distribution has been shown to vary significantly with the binary orbital eccentricity  $e_b$  and mass ratio  $q_b$  (D’Orazio et al. 2024). Here, we show that this variability is additionally sensitive to large-scale gas distribution. For an equal-mass, circular binary, rings exhibit clean, robust accretion variability at a frequency  $\sim 0.1\Omega_b$  (Fig. 3, left panels); the infinite disk dominant frequency is  $\sim 0.2\Omega_b$  (Fig. 3, right panels).

If circular binaries are surrounded by infinite disks, their variability may be the more difficult to detect. Lomb-Scargle or FFT analysis performed on short ( $\sim$ year) intervals of available timeseries data may not produce a high enough signal-to-noise ratio to identify a dominant frequency (Cocchiararo et al. 2024). Figure 3 suggests that periodograms of CBRs may be much cleaner, especially as  $\mathcal{M}$  increases.

Periodic signals from binaries in quasars are likely obscured by the stochastic variability inherent to AGN emission (Graham et al. 2017). Because of this, we caution the use of the Lomb-Scargle periodogram (LSP) to derive periodicity from light curves (LCs) of binary candidates. Lin et al. (2025) showed that the algorithm struggles with non-sinusoidal time series data representing binary signatures in quasars. In particular, sawtooth-like variability was detected for only a fraction (1.1%) of idealized light curves compared to sinusoidal signals (28.1%). Here we find that the enhanced eccentricity of disks evolved from circumbinary rings contributes to a new mode of accretion variability, resembling a  $\sim$ triangular wave pattern. The accuracy of the LSP for triangular signatures is yet to be tested.

### 5.2. *Dark Binary Mergers in Quasars*

We have found that the regime of suppressed accretion onto SMBHBs is robust to varying initial gas distribution in disk and ring initial conditions. As a result, we posit that cold gas may produce significantly weaker EM emission even if radial gas trajectories form a ring of gas at close encounter with the binary. This may limit prospects for detecting an EM-counterpart to SMBHB mergers, as such mergers may occur in the absence of surrounding gas. However, following binary coalescence, viscous inflow of the circumbinary gas is expected to produce a luminous AGN turn-on (Milosavljević & Phinney 2005; Tanaka et al. 2010; Shapiro 2010) that may be observable only a few years after the GW-driven merger (Tanaka & Menou 2010). Studying the lasting changes in AGN variability in so-called changing-look inspirals (CLIs) may reveal features of circumbinary disk interaction including gas temperature, viscosity and binary mass ratio (Zrake et al. 2025).

We have shown that, as the accretion suppression factor increases, the gas exerts increasingly negative torques on the binary (Figure 2; in agreement with Tiede et al. 2020). This may imply an efficient channel for the formation of massive black holes from mergers of lower mass (including stellar-mass) black hole binaries enabled by circumbinary disks. Gas-driven mergers, while likely EM-faint, may be a significant contributor to the GW background (Agazie et al. 2023).

### 5.3. *Quasi-Periodic Eruptions from Intermediate-Mass Black Hole Binaries*

Given the robustness of suppressed accretion in the high- $\mathcal{M}$  regime, we might expect the dominant source of variability to be from the inner CBD instead of accreting minidisks. Our simulations show that, even in this regime, rejected streams can shock heat the cavity wall and radiate in the UV or soft X-ray (Westernacher-Schneider et al. 2022). Recently, a number of galactic nuclei have been detected emitting bursts of soft X-rays in so-called quasi-periodic eruptions (QPEs) with periods ranging from hours to weeks (Miniutti et al. 2019; Giustini et al. 2020; Arcodia et al. 2021; Arcodia et al. 2024; Guolo et al. 2024; Nicholl et al. 2024). The dominant explanation has been a (stellar) body colliding with the accretion disk on a misaligned orbital plane (e.g. Linial et al. 2025). We propose a variation of the Nicholl et al. (2024) picture, in which a ring of gas is formed around a binary by tidal disruption of a star or infall of low angular momentum gas, and gas streams rejected by the binary impact the inner cavity wall and radiate quasi-periodically. If QPEs were instead sourced by stream impacts in circumbinary accretion flows, we

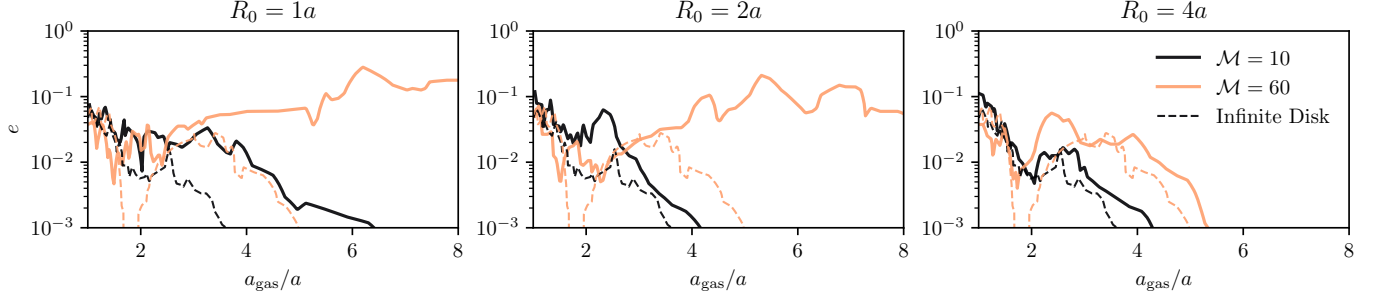


**Figure 4.** Eccentricity  $e = (\bar{e}_1^2 + \bar{e}_2^2)^{1/2}$  of the circumbinary gas binned by semi-major axis of the gas orbit,  $a_{\text{gas}}$ . The distributions are time-averaged at around  $t \approx 300$  orbits.

would expect periodic luminous bursts at twice the binary orbital frequency.

We can constrain the number of BHs with QPE-like periods using future LISA event rates  $\mathcal{R}_0$ , which provide an estimate for the rate of BHB mergers with a given mass. Here we consider intermediate-mass ( $M \sim 10^4 M_{\odot}$ ) black hole binaries (IMBHBs). From the derivation in Appendix A, we find that the number of candidate IMBHBs that could be QPE sources is

$$N \approx 4 \times 10^7 \left( \frac{\mathcal{R}_0}{1 \text{ yr}^{-1}} \right) \left( \frac{M}{10^4 M_{\odot}} \right)^{-5/3} \left( \frac{P}{13.3 \text{ days}} \right)^{8/3}, \quad (4)$$

where a period of 13.3 days corresponds to the widest binary with inspiral still dominated by GW emission. For an estimated merger rate of  $\mathcal{R}_0 \sim 1 \text{ yr}^{-1}$  (Fragione et al. 2022), the scaling given in Eq. (4) implies a raw population of order  $\sim 10^7$  IMBHBs with  $M \sim 10^4 M_{\odot}$  and periods in the QPE range. Eq. (4) also estimates a population of  $\sim 10^7$  IMBHBs with  $M \sim 10^5 M_{\odot}$  and  $P \lesssim 2$  months, which may be more easily detectable by LSST given its lower temporal cadence.

We note that only a fraction  $f_{\text{gas}}$  of binaries are surrounded by a gaseous environment, so the number of luminous binaries is better approximated by  $f_{\text{gas}}N$ . However, given the large raw population  $N$ , the number of detectable binaries remains significant even if  $f_{\text{gas}}$  is on the order of 1%.

#### 5.4. Supermassive Black Hole Binaries in Low-Luminosity Active Galactic Nuclei

AGN manifest across a wide spectrum of accretion flows, spanning super-Eddington accretion rates to highly inefficient, advection-dominated flows in low-luminosity AGN (LLAGN). Most AGN identified in nearby galaxies have optical signatures of nuclear activity in the form of low-ionization nuclear emission line regions (LINERs) which have been linked to LLAGN accreting far below the Eddington limit (Ho et al. 1997; Ho 1999; Terashima et al. 2000; Terashima & Wilson 2003;

Dudik et al. 2009; González-Martín et al. 2009). LINERs are produced by hot, collisionally excited species (e.g. O I, O II, S II and N II) with low ionization fractions and thus point to low UV ionizing flux from the central AGN engine (see Márquez et al. 2017 for review).

Inefficiently-accreting SMBHBs may have similar observational properties as LLAGN with LINER emission. In these systems, inefficient stream capture starves the accreting minidisks and thus suppresses their UV/optical emission. The lack of luminous minidisks may therefore lead to weak or absent broad line regions and a spectrum dominated by low-ionization transitions. Thus SMBHBs may resemble LINERs but with optical periodic variability at twice the binary frequency due to rejected streams shock heating the cavity wall. Compiling a catalog of LINERs and searching for optical variability with LSST may be a promising method to detect binary activity in LLAGN.

While this work does not account for magnetic fields, recent magnetohydrodynamic (MHD) simulations suggest that toroidally magnetized CBDs can produce magnetically arrested (MAD) accretion flows, in which large-scale poloidal flux accumulates around each black hole (Most & Wang 2025). The Blandford-Znajek process (Blandford & Znajek 1977) can then power dual relativistic jets from the cavity, producing radio and X-ray emission. Hence, non-accreting SMBHBs may appear as radio-loud, X-ray-bright but UV/optical-faint AGN with LINER spectra as a result of low UV ionizing flux.

#### 5.5. Asymmetric Double-Peaked Line Emission

When observed near edge-on, accretion disks emit a double-peaked line profile as a result of Doppler shift from gas approaching and receding at opposite sides of the disk (Eracleous & Halpern 1994; Eracleous et al. 1995). While circular disks exhibit approximately symmetric peaks, eccentric disks can produce enhanced asymmetry in relative strength as well as frequency separation of the peaks (Eracleous et al. 1995). Disk eccentricity has been proposed as a possible explanation for asymmetric double-peaks in AGN line profiles (Strateva

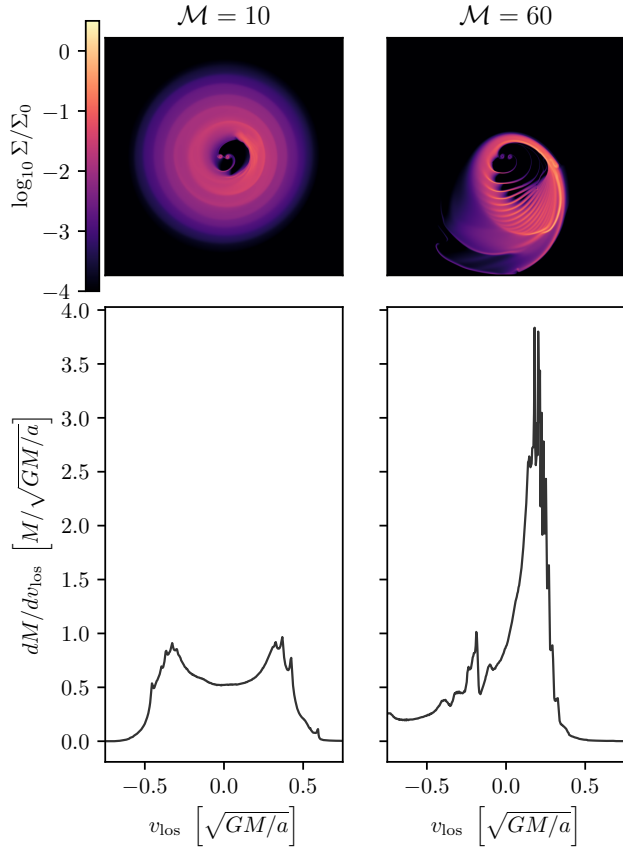


**Figure 5.** (Top) Density snapshots of ring  $R_0 = 2a$  and  $\mathcal{M} = \{10, 60\}$  at similar phases of precession. (Bottom) Corresponding velocity line profiles along the line of sight (LOS) chosen along the positive  $x$ -direction.

et al. 2003) and from disks evolved from TDEs (Wevers et al. 2022). In the latter, the extreme eccentricity of the disk ( $e = 0.91 \pm 0.01$ ) allows for measurement of the time-evolution of the double-peaks during the course of the disk’s precession on  $\sim$ week timescales.

We have shown that CBD eccentricity growth is suppressed by infinite disks that supply angular momentum to the inner circumbinary gas. Figure 4 shows that these extended disks saturate at an orbital eccentricity of  $e \simeq 0.05$ , even for higher  $\mathcal{M}$ . CBRs saturate at a significantly higher orbital eccentricity; gas in ring  $R_0 = 1a$  peaks just above  $e \simeq 0.3$ , and the peak saturation eccentricity rises for higher  $\mathcal{M}$ . Figure 5 illustrates the higher disk asymmetry for higher  $\mathcal{M}$ . The density plots (top panels) show the difference in large-scale disk eccentricity from rings of different  $\mathcal{M}$ . For the  $\mathcal{M} = 10$  ring, the significant pressure support in the gas has a circularizing effect. More frequent collisions between particles preferentially produces large deviations in azimuthal velocity, causing the gas to spread radially (Frank et al. 2002).

At  $\mathcal{M} = 60$  this effect is weak relative to the ECI. As a result the gas settles into a disk with significant eccentricity, creating a large asymmetry in velocity at orbital apsides. The distribution  $dM/dv_{\text{los}}$ , where  $v_{\text{los}}$  is the velocity along the chosen line of sight, illustrates how the eccentricity of the disk would manifest in an observed line profile. While the double-peaked line profile of  $\mathcal{M} = 10$  resembles that of a circular accretion disk, the asymmetric  $\mathcal{M} = 60$  profile is a potential signature of the eccentric disk.

In the elliptical disk model outlined by Eracleous et al. (1995), eccentricity affects both the separation and relative strength of double-peaked Balmer line emission profiles of AGN (see Fig. 3 in Eracleous et al. 1995). Stratéva et al. (2003) show that eccentricity as low as  $e \simeq 0.2$  could explain observed asymmetry in a sample of AGNs from the Sloan Digital Sky Survey, with some candidates suggesting an even more extreme  $e \simeq 0.8$ . If disk eccentricity in AGN is indeed driven by binaries, our findings indicate that the initial circumbinary ring must be of very small extent, with a radius comparable to the binary’s semimajor axis. Our measured disk eccentricities are high enough to explain observed asymmetry in accretion disk line emission (Stratéva et al. 2003), if this asymmetry is indeed the result of disk eccentricity as opposed to other features such as warps, spiral shocks, or temperature variability.

## 6. SUMMARY

Stellar and black hole binaries are shaped by their coupled interaction with gaseous environments, dictating their dynamical evolution and electromagnetic detectability. Previous works have largely studied relatively ‘thick’ circumbinary disks (CBDs) with aspect ratio  $h/r \sim \mathcal{M}^{-1} = 0.1$  and ‘infinite’ extent. Using high-resolution hydrodynamics simulations, we studied the viscous evolution of a finite circumbinary ring (CBR) as it spreads to form a CBD around a circular, equal-mass binary. Our suite of simulations spans ring radii in the range  $R_0 = 1a - 4a$ , capturing the limit in which the infinite disk approximation is valid; and Mach numbers  $\mathcal{M} = 10 - 60$ , to probe the dynamical properties of truly ‘thin’ disks. We summarize our findings below.

We have found that accretion dynamics are insensitive to large-scale disk structure, and both finite and infinite disks exhibit suppressed accretion onto the binary for higher  $\mathcal{M}$ . While the degree of accretion suppression is sensitive to viscosity prescription, our results suggest that these systems may produce reduced accretion-driven electromagnetic luminosity. A natural consequence of this accretion suppression is gas-driven binary inspiral induced by cold disks, with thinner disks

driving faster inspiral. We comment on the possibility that inefficiently-accreting SMBHBs may be responsible for weak accretion flows inferred from observations of LINER spectra in low-luminosity AGN. We show that gas surrounding IMBHBs may still show variability as QPEs sourced by gas streams rejected by the binary shocking the circumbinary cavity wall.

CBRs exhibit novel accretion periodicity, with accretion rate time series resembling quasi-triangular waves as opposed to the fiducial sawtooth pattern. CBRs surrounding circular, equal-mass binaries show lump-mediated accretion at a frequency  $\sim 0.1\Omega_b$ . This frequency is largely insensitive to  $\mathcal{M}$ . If CBRs represent a common configuration for circumbinary gas distribution, our results indicate that the associated accretion periodicity (for circular, equal-mass binaries) may be less noisy when recovered from quasar light curves. However, we caution the use of the Lomb-Scargle periodogram in future searches for binary signatures due to its bias against non-sinusoidal variability.

Smaller rings ( $R_0 = 1a$ ) evolve to disks with enhanced orbital eccentricity peaking at  $e \simeq 0.3$ . Rings of larger radius ( $R_0 = 4a$ ) viscously evolve to a structure resem-

bling an infinite disk, and thus saturate at  $e \simeq 0.05$ . We find that our measurements of disk eccentricity could explain inferred AGN disk asymmetry if the AGN hosts a central binary initially surrounded by a ring of sufficiently finite extent.

<sup>1</sup> The authors thank Zoltán Haiman, Magdalena Siwek  
<sup>2</sup> and Itai Linial for useful discussions. This work is sup-  
<sup>3</sup> ported by the National Aeronautics and Space Admin-  
<sup>4</sup> istration (NASA) under Grant No. 80NSSC22K0822 is-  
<sup>5</sup> sued through the Astrophysics Theory Program of the  
<sup>6</sup> Science Mission Directorate. Resources supporting this  
<sup>7</sup> work were provided by the NASA High-End Computing  
<sup>8</sup> (HEC) Program through the NASA Advanced Super-  
<sup>9</sup> computing (NAS) Division at Ames Research Center.  
<sup>10</sup> This work was supported in part through the NYU IT  
<sup>11</sup> High Performance Computing resources, services, and  
<sup>12</sup> staff expertise.

*Software:* JAX (Bradbury et al. 2018), astropy, matplotlib, pandas, SciPy.

## APPENDIX

### A. ESTIMATING BLACK HOLE BINARY POPULATIONS WITH LISA EVENT RATES

Our goal is to use future LISA event rates to constrain the number of intermediate-mass ( $M \sim 10^4 M_\odot$ ) black hole binaries (IMBHBs) with periods consistent with observed QPEs ( $P \sim$  hours – weeks). The following estimate is valid as long as the inspiral of the IMBHB is GW-dominated, i.e. if the characteristic inspiral inspiral time  $\tau$  is less than a Salpeter time  $t_{\text{sal}} = 4.5 \times 10^7$  years. The period of the binary orbit is  $P = 2\pi\sqrt{a^3/(GM)}$ . Equivalently, we can write  $a = (GM)^{1/3}(2\pi)^{-2/3}P^{2/3}$ . Assuming a circular, equal-mass binary, the inspiral time is given by Eq (5.9) from Peters (1964),

$$\begin{aligned}\tau &= a_0^4 \frac{5}{64} \frac{c^5}{G^3 M^3} \\ &= \left( \frac{5}{64} \right) (2\pi)^{-8/3} c^5 (GM)^{-5/3} P^{8/3},\end{aligned}$$

which can be rearranged to solve for the initial period  $P$  given an inspiral time  $\tau$ ,

$$\begin{aligned}P &= 2\pi\tau^{3/8} \left( \frac{5}{64} \right)^{-3/8} c^{-15/8} (GM)^{5/8} \\ &= 13.3 \text{ days} \left( \frac{M}{10^4 M_\odot} \right)^{5/3} \left( \frac{\tau}{4 \times 10^7 \text{ yr}} \right)^{3/8}.\end{aligned}\quad (\text{A1})$$

Let  $N(P, t)$  be the number of IMBHBs with periods less than  $P$ . Assuming a stationary population,  $\dot{N} = 0$ . The rate of mergers is

$$\mathcal{R}_0 \equiv \dot{P} \frac{dN}{dP},$$

where  $\mathcal{R}_0$  can be probed experimentally by LISA. Here  $\mathcal{R}_0$  is also the “flux” of  $n \equiv \frac{dN}{dP}$  where

$$\frac{\partial n}{\partial t} + \frac{\partial f}{\partial P} = 0,$$

is an advection equation for  $n$ ;  $f(P) \equiv \dot{P}n(p)$ . In steady-state  $f(P) = \mathcal{R}_0$  and  $n(P) = \mathcal{R}_0/\dot{P}$ .

Taking the time derivative of  $P$ ,

$$\dot{P} = 6\pi^2 P^{-1} \frac{a^2}{GM} \dot{a}.$$

For an equal-mass, circular binary, Peters (1964) Eq. (5.9) gives

$$\dot{a} = -\frac{16}{5} \frac{G^3 M^3}{c^5 a^3}$$

Then, we have

$$\dot{P} = -\left(\frac{96}{5}\right) 2^{2/3} \pi^{8/3} \frac{(GM)^{5/3}}{c^5} P^{-5/3}.$$

The binary population is

$$\begin{aligned} N(P) &= \int_0^P n(P') dP' \\ &\approx 4 \times 10^7 \left(\frac{\mathcal{R}_0}{1 \text{ yr}^{-1}}\right) \left(\frac{M}{10^4 M_\odot}\right)^{-5/3} \left(\frac{P}{13.3 \text{ days}}\right)^{8/3}. \end{aligned} \quad (\text{A2})$$

## REFERENCES

Agazie, G., Anumarpudi, A., Archibald, A. M., et al. 2023, *The Astrophysical Journal Letters*, 951, L8, doi: [10.3847/2041-8213/acdac6](https://doi.org/10.3847/2041-8213/acdac6)

Arcodia, R., Merloni, A., Nandra, K., et al. 2021, *Nature*, 592, 704, doi: [10.1038/s41586-021-03394-6](https://doi.org/10.1038/s41586-021-03394-6)

Arcodia, R., Liu, Z., Merloni, A., et al. 2024, *A&A*, 684, A64, doi: [10.1051/0004-6361/202348881](https://doi.org/10.1051/0004-6361/202348881)

Bate, M. R., Bonnell, I. A., & Bromm, V. 2003, *Monthly Notices of the Royal Astronomical Society*, 339, 577, doi: [10.1046/j.1365-8711.2003.06210.x](https://doi.org/10.1046/j.1365-8711.2003.06210.x)

Begelman, M. C., Blandford, R. D., & Rees, M. J. 1980, *Nature*, 287, 307, doi: [10.1038/287307a0](https://doi.org/10.1038/287307a0)

Blandford, R. D., & Znajek, R. L. 1977, *MNRAS*, 179, 433, doi: [10.1093/mnras/179.3.433](https://doi.org/10.1093/mnras/179.3.433)

Borchert, E. M. A., Price, D. J., Pinte, C., & Cuello, N. 2022, *Monthly Notices of the Royal Astronomical Society*, 517, 4436, doi: [10.1093/mnras/stac2872](https://doi.org/10.1093/mnras/stac2872)

Bradbury, J., Frostig, R., Hawkins, P., et al. 2018, *JAX: composable transformations of Python+NumPy programs*, 0.3.13. <http://github.com/jax-ml/jax>

Cocchiararo, F., Franchini, A., Lupi, A., & Sesana, A. 2024, *Astronomy & Astrophysics*, 691, A250, doi: [10.1051/0004-6361/202449598](https://doi.org/10.1051/0004-6361/202449598)

Coughlin, E. R., Armitage, P. J., Nixon, C., & Begelman, M. C. 2016, *Monthly Notices of the Royal Astronomical Society*, 465, 3840, doi: [10.1093/mnras/stw2913](https://doi.org/10.1093/mnras/stw2913)

Coughlin, E. R., Armitage, P. J., Nixon, C., & Begelman, M. C. 2017, *MNRAS*, 465, 3840, doi: [10.1093/mnras/stw2913](https://doi.org/10.1093/mnras/stw2913)

Dempsey, A. M., Muñoz, D., & Lithwick, Y. 2020, *ApJL*, 892, L29, doi: [10.3847/2041-8213/ab800e](https://doi.org/10.3847/2041-8213/ab800e)

Dittmann, A. J., & Ryan, G. 2022, *MNRAS*, 513, 6158, doi: [10.1093/mnras/stac935](https://doi.org/10.1093/mnras/stac935)

Dosopoulou, F., & Antonini, F. 2017, *The Astrophysical Journal*, 840, 31, doi: [10.3847/1538-4357/aa6b58](https://doi.org/10.3847/1538-4357/aa6b58)

Dotti, M., Colpi, M., Haardt, F., & Mayer, L. 2007, *MNRAS*, 379, 956, doi: [10.1111/j.1365-2966.2007.12010.x](https://doi.org/10.1111/j.1365-2966.2007.12010.x)

Duchêne, G., & Kraus, A. 2013, *Annual Review of Astronomy and Astrophysics*, 51, 269, doi: <https://doi.org/10.1146/annurev-astro-081710-102602>

Dudik, R. P., Satyapal, S., & Marcu, D. 2009, *ApJ*, 691, 1501, doi: [10.1088/0004-637X/691/2/1501](https://doi.org/10.1088/0004-637X/691/2/1501)

Duffell, P. C., Dittmann, A. J., D’Orazio, D. J., et al. 2024, *The Astrophysical Journal*, 970, 156, doi: [10.3847/1538-4357/ad5a7e](https://doi.org/10.3847/1538-4357/ad5a7e)

Duquennoy, A., & Mayor, M. 1991, *A&A*, 248, 485

D’Orazio, D. J., Duffell, P. C., & Tiede, C. 2024, *The Astrophysical Journal*, 977, 244, doi: [10.3847/1538-4357/ad938b](https://doi.org/10.3847/1538-4357/ad938b)

El-Badry, K., Rix, H.-W., & Heintz, T. M. 2021, *MNRAS*, 506, 2269, doi: [10.1093/mnras/stab323](https://doi.org/10.1093/mnras/stab323)

Eracleous, M., & Halpern, J. P. 1994, *ApJS*, 90, 1, doi: [10.1086/191856](https://doi.org/10.1086/191856)

Eracleous, M., Livio, M., Halpern, J. P., & Storchi-Bergmann, T. 1995, *ApJ*, 438, 610, doi: [10.1086/175104](https://doi.org/10.1086/175104)

Fragione, G., Loeb, A., Kocsis, B., & Rasio, F. A. 2022, *The Astrophysical Journal*, 933, 170, doi: [10.3847/1538-4357/ac75d0](https://doi.org/10.3847/1538-4357/ac75d0)

Frank, J., King, A., & Raine, D. 2002, *Accretion Power in Astrophysics*, 3rd edn. (Cambridge University Press)

Giustini, M., Miniutti, G., & Saxton, R. D. 2020, *A&A*, 636, L2, doi: [10.1051/0004-6361/202037610](https://doi.org/10.1051/0004-6361/202037610)

Goicovic, F. G., Cuadra, J., Sesana, A., et al. 2016, *MNRAS*, 455, 1989, doi: [10.1093/mnras/stv2470](https://doi.org/10.1093/mnras/stv2470)

González-Martín, O., Masegosa, J., Márquez, I., Guainazzi, M., & Jiménez-Bailón, E. 2009, *A&A*, 506, 1107, doi: [10.1051/0004-6361/200912288](https://doi.org/10.1051/0004-6361/200912288)

Graham, M. J., Djorgovski, S. G., Drake, A. J., et al. 2017, *Monthly Notices of the Royal Astronomical Society*, 470, 4112–4132, doi: [10.1093/mnras/stx1456](https://doi.org/10.1093/mnras/stx1456)

Grudić, M. Y., Guszejnov, D., Offner, S. S. R., et al. 2022, *Monthly Notices of the Royal Astronomical Society*, 512, doi: [10.1093/mnras/stac526](https://doi.org/10.1093/mnras/stac526)

Guerra-Alvarado, O. M., van der Marel, N., Williams, J. P., et al. 2025, *Astronomy & Astrophysics*, 696, A232, doi: [10.1051/0004-6361/202453338](https://doi.org/10.1051/0004-6361/202453338)

Guolo, M., Pasham, D. R., Zajaček, M., et al. 2024, *Nature Astronomy*, 8, 347, doi: [10.1038/s41550-023-02178-4](https://doi.org/10.1038/s41550-023-02178-4)

Ho, L. C. 1999, *Advances in Space Research*, 23, 813, doi: [https://doi.org/10.1016/S0273-1177\(99\)00211-2](https://doi.org/10.1016/S0273-1177(99)00211-2)

Ho, L. C., Filippenko, A. V., Sargent, W. L. W., & Peng, C. Y. 1997, *ApJS*, 112, 391, doi: [10.1086/313042](https://doi.org/10.1086/313042)

Lin, A., Charisi, M., & Haiman, Z. 2025, Lomb-Scargle periodograms struggle with non-sinusoidal supermassive BH binary signatures in quasar lightcurves. <https://arxiv.org/abs/2505.14778>

Linial, I., Metzger, B. D., & Quataert, E. 2025, *The Astrophysical Journal*, 991, 147, doi: [10.3847/1538-4357/adfa0e](https://doi.org/10.3847/1538-4357/adfa0e)

Lubow, S. H. 1991, *ApJ*, 381, 259, doi: [10.1086/170647](https://doi.org/10.1086/170647)

MacFadyen, A. I., & Milosavljević, M. 2008, *ApJ*, 672, 83, doi: [10.1086/523869](https://doi.org/10.1086/523869)

Merritt, D., & Milosavljević, M. 2005, *Living Reviews in Relativity*, 8

Milosavljević, M., & Phinney, E. S. 2005, *ApJ*, 622, L93, doi: [10.1086/429618](https://doi.org/10.1086/429618)

Miniutti, G., Saxton, R. D., Giustini, M., et al. 2019, *Nature*, 573, 381, doi: [10.1038/s41586-019-1556-x](https://doi.org/10.1038/s41586-019-1556-x)

Most, E. R., & Wang, H.-Y. 2025, *Phys. Rev. D*, 111, L081304, doi: [10.1103/PhysRevD.111.L081304](https://doi.org/10.1103/PhysRevD.111.L081304)

Muñoz, D. J., Lai, D., Kratter, K., & Miranda, R. 2020, *ApJ*, 889, 114, doi: [10.3847/1538-4357/ab5d33](https://doi.org/10.3847/1538-4357/ab5d33)

Muñoz, D. J., Miranda, R., & Lai, D. 2019, *ApJ*, 871, 84, doi: [10.3847/1538-4357/aaf867](https://doi.org/10.3847/1538-4357/aaf867)

Márquez, I., Masegosa, J., González-Martín, O., et al. 2017, *Frontiers in Astronomy and Space Sciences*, Volume 4 - 2017, doi: [10.3389/fspas.2017.00034](https://doi.org/10.3389/fspas.2017.00034)

Nicholl, M., Pasham, D. R., Mummery, A., et al. 2024, Quasi-periodic X-ray eruptions years after a nearby tidal disruption event. <https://arxiv.org/abs/2409.02181>

Peters, P. C. 1964, *Phys. Rev.*, 136, B1224, doi: [10.1103/PhysRev.136.B1224](https://doi.org/10.1103/PhysRev.136.B1224)

Qian, K., Li, J., & Lai, D. 2024, *The Astrophysical Journal*, 962, 143, doi: [10.3847/1538-4357/ad1b53](https://doi.org/10.3847/1538-4357/ad1b53)

Raghavan, D., McAlister, H. A., Henry, T. J., et al. 2010, *ApJS*, 190, 1, doi: [10.1088/0067-0049/190/1/1](https://doi.org/10.1088/0067-0049/190/1/1)

Ragusa, E., Lodato, G., & Price, D. J. 2016, *arXiv.org*, arXiv:1605.01730

Ryu, T., Perna, R., & Wang, Y.-H. 2022, *Monthly Notices of the Royal Astronomical Society*, 516, 2204–2217, doi: [10.1093/mnras/stac2316](https://doi.org/10.1093/mnras/stac2316)

Shakura, N. I., & Sunyaev, R. A. 1973, *A&A*, 24, 337

Shapiro, S. L. 2010, *PhRvD*, 81, 24019, doi: [10.1103/PhysRevD.81.024019](https://doi.org/10.1103/PhysRevD.81.024019)

Shi, J.-M., Krolik, J. H., Lubow, S. H., & Hawley, J. F. 2012, *ApJ*, 749, 118, doi: [10.1088/0004-637X/749/2/118](https://doi.org/10.1088/0004-637X/749/2/118)

Strateva, I. V., Strauss, M. A., Hao, L., et al. 2003, *The Astronomical Journal*, 126, 1720, doi: [10.1086/378367](https://doi.org/10.1086/378367)

Tanaka, T., Haiman, Z., & Menou, K. 2010, *The Astronomical Journal*, 140, 642, doi: [10.1088/0004-6256/140/2/642](https://doi.org/10.1088/0004-6256/140/2/642)

Tanaka, T., & Menou, K. 2010, *ApJ*, 714, 404, doi: [10.1088/0004-637X/714/1/404](https://doi.org/10.1088/0004-637X/714/1/404)

Terashima, Y., Ho, L. C., & Ptak, A. F. 2000, *ApJ*, 539, 161, doi: [10.1086/309234](https://doi.org/10.1086/309234)

Terashima, Y., & Wilson, A. S. 2003, *ApJ*, 583, 145, doi: [10.1086/345339](https://doi.org/10.1086/345339)

Tiede, C., Zrake, J., MacFadyen, A., & Haiman, Z. 2020, *ApJ*, 900, 43, doi: [10.3847/1538-4357/aba432](https://doi.org/10.3847/1538-4357/aba432)

Tiede, C., Zrake, J., MacFadyen, A., & Haiman, Z. 2025, The Astrophysical Journal, 984, 144, doi: [10.3847/1538-4357/adc727](https://doi.org/10.3847/1538-4357/adc727)

Volonteri, M., Haardt, F., & Madau, P. 2003, ApJ, 582, 559, doi: [10.1086/344675](https://doi.org/10.1086/344675)

Westernacher-Schneider, J. R., Zrake, J., MacFadyen, A., & Haiman, Z. 2022, PhRvD, 106, 103010, doi: [10.1103/PhysRevD.106.103010](https://doi.org/10.1103/PhysRevD.106.103010)

Wevers, Nicholl, M., Guolo, M., et al. 2022, A&A, 666, A6, doi: [10.1051/0004-6361/202142616](https://doi.org/10.1051/0004-6361/202142616)

Yu, F., & Lai, D. 2025, The Astrophysical Journal, 993, 88, doi: [10.3847/1538-4357/ae032b](https://doi.org/10.3847/1538-4357/ae032b)

Zrake, J., Clyburn, M., & Feyan, S. 2025, MNRAS, 537, 3620, doi: [10.1093/mnras/staf171](https://doi.org/10.1093/mnras/staf171)